A&A 466, 31–40 (2007)
DOI: 10.1051/0004-6361:20065170

Astronomy & Astrophysics

The HELLAS2XMM survey

VIII. Optical identifications of the extended sample⋆,⋆⋆

F. Cocchia[1,2,3], F. Fiore[1], C. Vignali[4,5], M. Mignoli[5], M. Brusa[6], A. Comastri[5], C. Feruglio[1,2], A. Baldi[7], N. Carangelo[8], P. Ciliegi[5], V. D'Elia[1], F. La Franca[9], R. Maiolino[1,10], G. Matt[9], S. Molendi[8], G. C. Perola[9], and S. Puccetti[1,11]

[1] INAF – Osservatorio Astronomico di Roma, via Frascati 33, Monteporzio-Catone (RM) 00040, Italy
e-mail: cocchia@brera.mi.astro.it
[2] Dipartimento di Fisica, Università di Roma Tor Vergata, via della Ricerca Scientifica 1, 00133 Rome, Italy
[3] INAF – Osservatorio Astronomico di Brera, via Brera 28, 20121 Milano, Italy
[4] Dipartimento di Astronomia, Università di Bologna, via Ranzani 1, 40127 Bologna, Italy
[5] INAF – Osservatorio Astronomico di Bologna, via Ranzani 1, 40127 Bologna, Italy
[6] Max Planck Institüt für Extraterrestrische Physik (MPE), Giessenbachstr. 1, 85748 Garching, Germany
[7] Harvard-Smithsonian Center for Astrophysics (CfA), 60 Garden str, Cambridge 02138 MA, USA
[8] INAF – IASF, via Bassini 15, 20133 Milano, Italy
[9] Dipartimento di Fisica, Università Roma Tre, via della Vasca Navale 84, 00146 Roma, Italy
[10] INAF – Osservatorio Astrofisico di Arcetri, Largo Enrico Fermi 5, 50125 Firenze, Italy
[11] ASI Science Data Center, ASDC c/o ESRIN, via G. Galilei, 00044 Frascati, Italy

Received 9 March 2006 / Accepted 1 December 2006

ABSTRACT

Aims. Hard X-ray, large-area surveys are a fundamental complement to ultra-deep, pencil-beam surveys in obtaining more complete coverage of the AGN luminosity-redshift plane and finding sizeable samples of "rare" AGN.
Methods. We present the results of the photometric and spectroscopic identification of 110 hard X-ray selected sources from 5 additional XMM-*Newton* fields, nearly doubling the original HELLAS2XMM sample. Their 2–10 keV fluxes cover the range 6×10^{-15}–4×10^{-13} erg cm^{-2} s^{-1} and the total area surveyed is ∼0.5 deg^2 at the bright flux limit. We spectroscopically identified 59 new sources, bringing the spectroscopic completeness of the full HELLAS2XMM sample to almost 70% over a total area of ∼1.4 deg^2 at the bright flux limit. We found optical counterparts for 214 out of the 232 X-ray sources of the full sample down to $R \sim 25$. We measured the flux and luminosity of the [OIII]λ5007 emission line for 59 of these sources.
Results. Assuming that most high X-ray-to-optical flux ratio sources are obscured QSOs, we used the full HELLAS2XMM sample and the CDF samples to estimate their $\log N - \log S$. We find obscured QSOs surface density of 45 ± 15 and 100–350 deg^{-2} down to flux limits of 10^{-14} and 10^{-15} erg cm^{-2} s^{-1}, respectively. At these flux limits, the fraction of X-ray-selected obscured QSOs turns out to be similar to that of unobscured QSOs. Since X-ray selection misses most Compton-thick AGN, the number of obscured QSOs may well outnumber the unobscured QSOs.
We find that hard X-ray selected AGNs with a detected [OIII] emission span a wide range of $L_{2-10\,\mathrm{keV}}/L_{[\mathrm{OIII}]}$ with a logarithmic median of 2.14 and interquartile range of 0.38. This is marginally higher than for a sample of optically selected AGNs (median 1.69 and interquatile range 0.30), suggesting that optically selected samples are at least partly incomplete and/or that [OIII] emission is not a perfect isotropic indicator of the nuclear power. The seven X-ray bright, optically normal galaxy (XBONG) candidates in the sample have $L_{2-10\,\mathrm{keV}}/L_{[\mathrm{OIII}]} \gtrsim 1000$, while their X-ray and optical luminosities and obscuring column density are similar to those of narrow-line AGNs in the same redshift interval (0.075–0.32). This suggests that, while the central engine of narrow-line AGNs and XBONGs looks similar, the narrow-line region in XBONGs could be strongly inhibited or obscured.

Key words. X-rays: diffuse background – surveys – galaxies: active – galaxies: evolution

1. Introduction

Deep *Chandra* and XMM-*Newton* hard X-ray surveys have been able to detect the sources making up the majority of the cosmic X-ray background (XRB) below 6–7 keV (Giacconi et al. 2002; Bauer et al. 2004; Moretti et al. 2003; Worsley et al. 2004; Brandt & Hasinger 2005). However, deep surveys cover only a fraction of a square degree of sky, making it difficult to find sizable samples of medium- and high-luminosity sources. To obtain a more complete coverage of the redshift-luminosity plane, which complements deep surveys, and to compute an accurate luminosity function over wide luminosity and redshift intervals a much larger area on the order of a few square degrees needs to be covered. Furthermore, large-area surveys can provide sizeable samples of "rare" objects. To these purposes, we

⋆ Based on observations collected at the European Southern Observatory, Prog. ID 67.A-0401, 68.A-0514, 69.A-0563 and 072.A-0633, and at the Telescopio Nazionale Galileo, Prog. ID 1_15_083. Based also on observations made with XMM-Newton, an ESA science mission.

⋆⋆ Tables 1, 3, 4 are only available in electronic form at the CDS via anonymous ftp to cdsarc.u-strasbg.fr (130.79.128.5) or via http://cdsweb.u-strasbg.fr/cgi-bin/qcat?J/A+A/466/31

are carrying out the HELLAS2XMM serendipitous survey using suitable XMM-*Newton* archival observations (Baldi et al. 2002). As a first step, we presented the optical identification of 122 hard X-ray selected sources detected in five XMM-*Newton* fields in Fiore et al. (2003, hereafter the 1dF sample). Here we report the results of the photometric and spectroscopic identification of 110 X-ray sources from five additional XMM-*Newton* fields (hereafter the HELLAS2XMM second source sample), nearly doubling the original HELLAS2XMM sample and bringing the total area surveyed to about 1.4 deg^2 at a flux limit of $\sim 10^{-13}$ erg cm^{-2} s^{-1}.

One of the most interesting findings of the optical identifications of the HELLAS2XMM sample, as well as of other hard X-ray selected *Chandra* and XMM-*Newton* surveys (see, e.g., ChaMP: Silverman et al. 2005; SEXSI: Eckart et al. 2005; CLASXS, CDFN, CDFS: Barger et al. 2005; CDFS, CDFN: Giacconi et al. 2002; Hasinger et al. 2003; XMM/2dF Georgakakis et al. 2004; HBS: Della Ceca et al. 2004) is the discovery that AGN activity spans a much wider range of properties than was thought based on optically and soft X-ray selected AGNs. Indeed, hard X-ray selection provides a more complete view of AGN activity, being more efficient in selecting sources possibly missed by selection in other bands, e.g., obscured and low-luminosity AGNs, several of which are left out in optical or soft X-ray selected samples. While most of the optically and soft X-ray selected AGNs have an X-ray-to-optical (R-band) flux ratio X/O[1] between 0.1 and 10 (see, e.g., Maccacaro et al. 1988; Laor et al. 1997; Hasinger et al. 1998; Mineo et al. 2000), XMM-*Newton* and *Chandra* hard X-ray surveys have selected AGNs with X-ray-to-optical flux ratio well outside this range. In particular, the HELLAS2XMM survey has detected both a population of relatively bright X-ray sources with faint optical counterparts (and thus characterized by high X/O values; Fiore et al. 2003) and several X-ray sources in otherwise inactive and optically bright galaxies (with relatively low X/O ratios; named X-ray bright, optically normal galaxies, XBONGs, Fiore et al. 2000; Comastri et al. 2002).

The former population includes about 15–20% of the sources selected in the 2–10 keV band to have X/O more than one order of magnitude higher than that of typical broad-line, type 1 AGNs. Based on optical spectroscopy (Fiore et al. 2003), optical-to-near-infrared colors (Mignoli et al. 2004), near-infrared (Maiolino et al. 2006), and X-ray spectroscopy (Perola et al. 2004), we concluded that the majority of the HELLAS2XMM sources with X/O $\gtrsim 10$ are optically obscured QSOs at $z \gtrsim 1$. At fainter X-ray and optical fluxes, the situation is less clear, mainly because most of the optical counterparts of the high X/O sources are inaccessible to optical spectroscopy even with 10 m-class telescopes.

The XBONGs, on the other hand, are found at low redshift ($\sim$0.1–0.3), with X-ray luminosities between 10^{42} and 10^{43} erg s^{-1}, bright optical counterparts ($R < 21$), thus relatively low X/O, and absorption-dominated optical spectra without strong nuclear emission (Comastri et al. 2002). It has been suggested that XBONGs selected in *Chandra* and XMM-*Newton* surveys are actually typical AGNs classified as normal galaxies just because of some observational biases (dilution of the nuclear spectrum by the host galaxy, inadequate set-up for optical spectroscopy in terms of wavelength range covered, signal-to-noise ratio, spatial resolution, see e.g. Moran et al. 2002; Severgnini et al. 2003; Georgantopoulos & Georgakakis 2005).

In this paper we present the optical identification follow-up observations of five additional fields of the HELLAS2XMM survey and focus the discussion on both the high X/O sources and the XBONGs, providing quantitative constraints to the space density of highly optically-obscured, high-luminosity QSOs and proposing a quantitative definition of XBONGs. The paper is organized as follows. Sections 2 and 3 present the results of the optical photometric and spectroscopic identifications of the HELLAS2XMM second-source sample. Section 4 discusses our main findings; and Sect. 5 reports our conclusions. An $H_0 = 70$ km s^{-1} Mpc^{-1}, $\Omega_{\rm M} = 0.3$, $\Omega_\Lambda = 0.7$ cosmology is adopted throughout.

2. Optical identifications

The HELLAS2XMM second-source sample includes sources detected in the 2–10 keV band in five XMM-*Newton* fields: A1835, IRAS13349+2438, GD153, Mrk421, BPM16274 (see Baldi et al. 2002, for details on the observations and X-ray data reduction). We have obtained relatively deep (exposure time 3–15 m per image, limiting magnitude $R = 24$–25) optical images for the majority of the sources in these five fields, using EFOSC2 at the ESO 3.6 m telescope, FORS1 at VLT, and DOLORES at the TNG.

We exclude from the following analysis those areas in the five fields not covered by R-band images. This, together with the fact that Mrk421 field has been observed in window mode and that a large-area centered on the A1835 cluster of galaxies has been excluded from the analysis, reduces the total area surveyed to about 0.5 deg^2. The total number of hard X-ray selected sources making the HELLAS2XMM second-source sample is 110, bringing the total number of sources in the full HELLAS2XMM sample with optical coverage to 232 in ten XMM-*Newton* fields.

Optical images were bias-subtracted, flat-field divided, and flux-calibrated using observations of standard stars acquired during each night. Optical and X-ray images were brought to a common astrometric reference frame using bright AGNs (from 5 to 15 AGNs per field). Typical systematic shifts were on the order of 1″, and the maximum shift was of $\sim$2″.

Source detection in the optical images was performed using the SExtractor package (Bertin et al. 1996) and we visually searched for optical counterparts of the X-ray selected sources within a conservative matching radius of 6 arcsec from the astrometrically-corrected X-ray centroid. For X-ray sources with multiple optical counterparts we provide the probability P of chance coincidence[2] in Table 1 (see also Brusa et al. 2003).

Optical counterparts brighter than $R \sim 24.5$ within $\sim$6″ from the X-ray position were found for 103 sources. There are two candidate counterparts for 15 of them inside the X-ray error-box. For each source, Table 1 gives the X-ray position, the position of the most likely optical counterpart (identified on the basis of its magnitude, displacement from the X-ray position and probability of chance coincidence, classification of the optical spectrum), the displacement between the X-ray and optical positions, the X-ray flux, and the R magnitude (or lower limit) of the optical counterpart. In three cases, more than one optical source might contribute to the detected X-ray emission (see notes to Table 1).

[1] X/O $= \log \frac{f_{\rm X}}{f_R} = \log f_{\rm X} + \frac{R}{2.5} + C$, where C depends on the chosen X-ray band and optical filter.

[2] $P = {\rm e}^{-\pi r^2 n(R)}$ where r is the X-ray-optical displacement and $n(R)$ the number counts of galaxies as a function of their magnitude from Metcalfe et al. (2001).

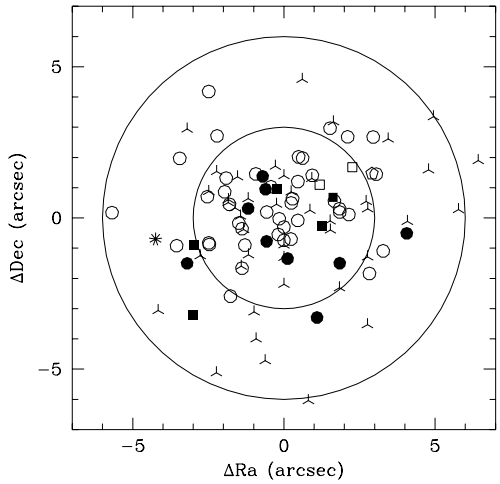

Fig. 1. The displacement between the X-ray position and the position of the nearest optical counterpart for the HELLAS2XMM second-source sample. Open circles = broad-line AGN; filled circles = narrow-line AGN; filled squares = emission-line galaxies; open squares = early-type galaxies; stars = stars; pentagons = groups/clusters of galaxies; skeleton triangles = unidentified objects. The two circles have radii of 3 and 6 arcsec.

The average displacement between the X-ray centroid and the position of the most likely optical counterparts is 2.4″ ± 1.4″. For ∼67% of the sources, the displacement is <3″ (see Fig. 1). These shifts are slightly worse than those found for the HELLAS2XMM 1dF sample (average displacement of 2.0″ ± 1.4″ and 80% of the sources within 3″, Fiore et al. 2003), most likely because the average off-axis angle (and therefore the average point spread function) of the sources in the second sample is higher than for the sources in the 1dF sample, due to the exclusion of the central parts of two fields (Mrk421 and A1835).

3. Optical spectroscopic redshifts and classification

Our main effort was to start to explore the region of high X/O values to obtain an optical spectroscopy that is as uniform as possible regarding the X-ray-to-optical flux ratio. This was roughly achieved up to X/O = 40, which corresponds to $R \sim 24$ for 2–10 keV fluxes of $\sim 10^{-14}$ erg cm^{-2} s^{-1}. Most of the HELLAS2XMM sources have higher X-ray flux than this figure.

Optical spectra of 59 out of the 110 sources with optical counterparts brighter than $R = 24$ were obtained using EFOSC2 at the ESO 3.6 m telescope, DOLORES at the TNG and FORS1 at the VLT/UT1 during 6 observing runs performed between August 2001 and March 2004. A total of 12 nights at the 3.6 m and TNG telescopes and ∼40 h of VLT time were devoted to this program.

Long-slit spectroscopy was carried out in the 3800–10 000 Å band with resolution between 7 and 13 Å. Data reduction was performed using both the MIDAS (Banse et al. 1983) and IRAF[3] packages. Wavelength calibrations were carried out by comparison with exposures of He-Ar, He, Ar, and Ne lamps. The flux calibration of the spectra was obtained using observations of spectro-photometric standard stars (Oke 1990) performed within a few hours of the spectroscopy for our sources.

Regardless of the optical spectra, our discriminant for supermassive black hole accretion is high X-ray luminosity; we classify a source as an AGN if it has an X-ray luminosity $\log L_{2-10\ \mathrm{keV}} \geq 42$. If a source has an X-ray luminosity $\log L_{2-10\ \mathrm{keV}} \geq 44$, we classify it as a QSO candidate. Following Fiore et al. (2003), objects with permitted emission lines broader than 2000 km s^{-1} (*FWHM*)[4] are classified type 1 AGN or QSO. Objects with narrower permitted emission lines than this threshold and strong (equivalent width $EW > 5$ Å) [OIII], MgII, NeV or CIV emission lines are classified as type 2 AGN. Objects with faint (equivalent width $EW < 5$ Å) [OIII] and/or strong [OII] or Hα and no high-ionization emission lines are classified as emission-line galaxies (ELGs). In one case the presence of broad emission lines in the optical spectrum cannot be excluded due to the insufficient quality of the spectrum, so the classification of the object is uncertain (see notes in Table 1). Objects without strong emission lines but with stellar absorption lines and a red continuum are classified as early type galaxies (ETGs, or XBONGs, as they are X-ray bright sources with optical spectra typical of early type galaxies). Table 1 gives the classification of the optical spectrum, the redshift, and the X-ray luminosity for each source.

The source breakdown includes: 41 broad-line AGNs (QSOs and Seyfert 1 galaxies, $\log L_{2-10\ \mathrm{keV}} > 44$, and $\log L_{2-10\ \mathrm{keV}} < 44$, respectively); 9 narrow-line AGNs (type 2 QSOs and Seyfert 2 galaxies); 5 emission-line galaxies, all with $\log L_{2-10\ \mathrm{keV}} > 42.7$ and therefore all probably hosting an AGN; 2 early-type galaxies, both with $\log L_{2-10\ \mathrm{keV}} > 42.0$ and, therefore, XBONG candidates, probably hosting an AGN; 1 group of galaxies; 1 star. In summary, 57 of the 59 sources with optical spectroscopy are associated with AGN emission, the majority (69%) are type 1 AGNs. This brings the number of confirmed AGNs in the full HELLAS2XMM sample to 155 out of 159 with a spectroscopic redshift.

The four panels of Fig. 2 show the redshift-luminosity plane and the redshift, R magnitude, X-ray-to-optical flux ratio histograms for the full HELLAS2XMM sample. The observed fraction of type 1 AGNs increases strongly with redshift, corresponding to ∼90% of the *whole* source population with a spectroscopic redshift higher than 1.5. Conversely, the fraction of type 1 AGNs decreases strongly with increasing X-ray-to-optical flux ratio and with the magnitude of the optical counterpart of the X-ray source, with only one of the eleven sources with $R \gtrsim 23.3$ and a spectroscopic redshift identified as a type 1 AGN (see Fiore et al. 2003; La Franca et al. 2005; Eckart et al. 2006; Silverman et al. 2005; Treister et al. 2005; Steffen et al. 2004, for similar results and more detailed discussions). This suggests that the lack of high-z type 2 AGNs in the sample of spectroscopically identified HELLAS2XMM sources (Fig. 2, upper right panel) can be probably due to the incompleteness of the sample: at $z \gtrsim 1.5$ the R-band magnitude of the optical counterparts of type 2 AGN is often beyond the spectroscopic limit of our sample ($R \sim 24$). Furthermore, even for objects brighter than the spectroscopic limit, the optical nucleus is so dim that the redshift determination is complex for the lack of observable lines, the so-called spectroscopic redshift desert at $z = 1.5-2$.

[3] IRAF is distributed by the National Optical Astronomy Observatories, which is operated by the Association of Universities for Research in Astronomy, Inc., under cooperative agreement with the National Science Fundation.

[4] Removing the instrumental broadening from the line profile, the adopted velocity threshold corresponds to an intrinsic *FWHM* of ∼1500 km s^{-1}.

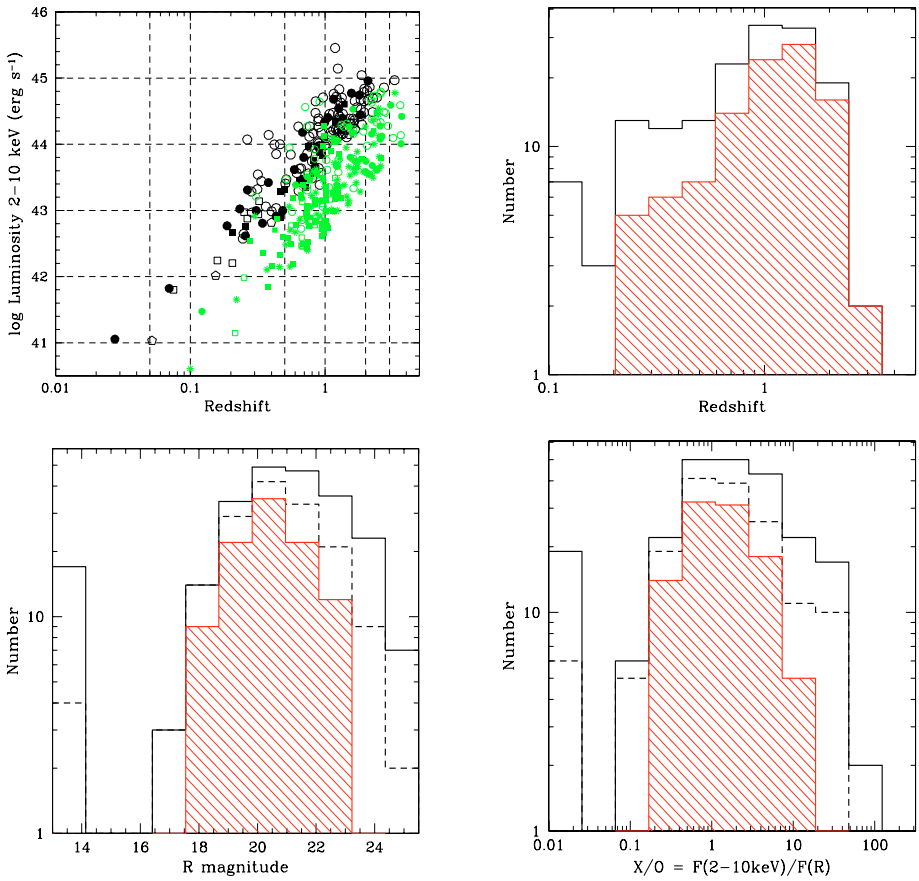

Fig. 2. a) *Upper left panel*: the 2–10 keV luminosity as a function of the redshift for the sources in the full HELLAS2XMM sample (black points) compared with the luminosity as a function of the redshift for CDFS+CDFN samples (smaller green points; data from Giacconi et al. 2002; Alexander et al. 2003; Barger et al. 2003; Szokoly et al. 2004). Stars are CDFS and CDFN sources with photometric redshifts. **b)** *Upper right panel*: the redshift distribution of the 159 sources with spectroscopic redshifts of the full HELLAS2XMM sample. The hatched histogram only refers to type 1 AGN and the continuous histogram to the source population with spectroscopic z. **c)** *Lower left panel*: the R magnitude distribution; **d)** *lower right panel*: the X-ray-to-optical flux ratio X/O distribution. In the **c)** and **d)** panels the hatched histograms only refer to type 1 AGN, the dashed histograms to the source population with spectroscopic z, the continuous histograms to the whole source population.

3.1. Optically obscured AGN

Following Fiore et al. (2003), we limit ourselves to considering two broad AGN categories: optically unobscured AGN, i.e. type 1, broad emission line AGN; and optically obscured AGN, i.e. non type 1 AGN, in which the nuclear optical emission is totally or partly reduced by dust and gas in the nuclear region and/or in the host galaxy. The fraction of optically obscured AGN with respect to the total number of identified X-ray sources is approximately 27% (16 out of 59 X-ray sources, see also the source breakdown). Two examples of such sources are reported in Fig. 3. The H$_\beta$ *FWHM* of GD153_236 (H2XMMJ125654.1+215318; z = 0.909, AGN2) is <1000 km s^{-1}. Faint [OII] and [OIII] emission is present in the spectrum of A1835_262 (H2XMMJ140130.8+024532; z = 0.746, ELG). This source is also obscured in the X-ray band, having a 0.5–2 keV flux less than 20 times the observed 2–10 keV flux; to be more quantitative, the X-ray spectral fit yields a rest frame $N_{\rm H}(z) \simeq 7.9^{+3.3}_{-2.2} \times 10^{22}$ cm^{-2}, fixing the spectral energy index α_E ($F(E) \propto E^{-\alpha_E}$) to 0.9. GD153_236 is less extreme in this regard, as the X-ray spectral fit yields a rest frame $N_{\rm H}(z) = 0.3^{+0.4}_{-0.3} \times 10^{22}$ cm^{-2}, fixing the spectral energy index α_E to 0.9. The 2–10 keV intrinsic luminosity is 1.10×10^{44} erg s^{-1} for A1835_262 and 1.59×10^{44} erg s^{-1} for GD153_236, making them obscured QSO candidates.

We are interested in finding a statistical method for selecting highly obscured QSO candidates among the still unidentified sample sources in order to estimate their surface density. To this purpose, we make use of observed quantities in the following, such as the observed-frame absorbing column $N_{\rm H}$ and the X/O ratio. We use the results of our spectroscopic identifications to calibrate and validate this statistical method.

The observed-frame absorbing column $N_{\rm H}(z = 0)$ (computed from the hardness ratios following Fiore et al. 2003) as a function of X/O for the full HELLAS2XMM sample is reported in Fig. 4 (left panel). We note that the part of the diagram at X/O > 8 and $\log N_{\rm H}(z = 0) > 21$ is mainly populated by narrow-line objects. More quantitatively, 16 out of the 20 objects with optical spectroscopy are, according to the definition of Fiore et al. (2003), optically obscured AGNs (i.e., 80 ± 20%).

Since the observed $\log N_{\rm H} = 21$ would correspond to a rest-frame column density of $\log N_{\rm H} = 21.5$ at $z = 1$, most of these AGNs, having redshifts $z \gtrsim 1$, are also X-ray obscured (see also Mainieri et al. 2002). The right panel of Fig. 4 shows X/O as a function of the 2–10 keV luminosity for the HELLAS2XMM full source sample. This figure clearly shows that most optically obscured AGN with X/O > 8 have high luminosities ($\log L$ (2–10 keV) > 44), highlighting the efficiency of a selection based on the observed X/O ratio to find highly obscured QSO candidates.

The number of spectroscopically identified sources in the HELLAS2XMM sample with $\log N_{\rm H}(0) > 21$, X/O > 8 and $\log L$(2–10 keV) > 44 is 17. Thirteen of these are optically obscured AGN, i.e. a fraction of 0.76 ± 0.25.

The diagram in the left panel of Fig. 5 shows the $N_{\rm H}(0)$ as a function of X/O ratio for the CDFS and CDFN sources (Giacconi et al. 2002; Alexander et al. 2003; Barger et al. 2003; Szokoly et al. 2004) selected by Fiore (2004) by having 2–10 keV fluxes larger than 10^{-15} erg cm^{-2} s^{-1} and off-axis angles lower than 10 arcmin. Unfortunately, most of the sources from these samples with X/O > 8 and $\log N_{\rm H}(z = 0) > 21$ do not

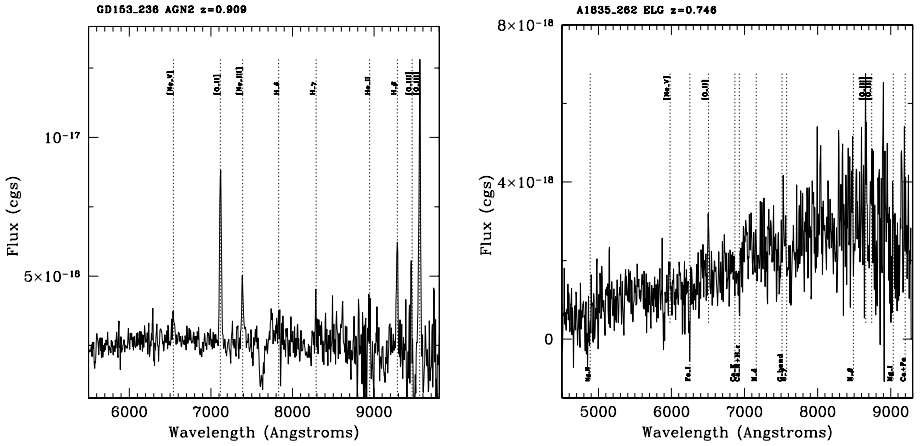

Fig. 3. The optical spectra of GD153_236 (H2XMMJ125654.1+215318) and A1835_262 (H2XMMJ140130.8+024532). Both spectra are classified as narrow emission-line objects based on the H_β *FWHM* (<1000 km s^{-1}, GD153_236), narrow [OII] and [OIII] emission, absence of broad permitted lines and high 2–10 keV luminosity (~10^{44} erg s^{-1} for both sources).

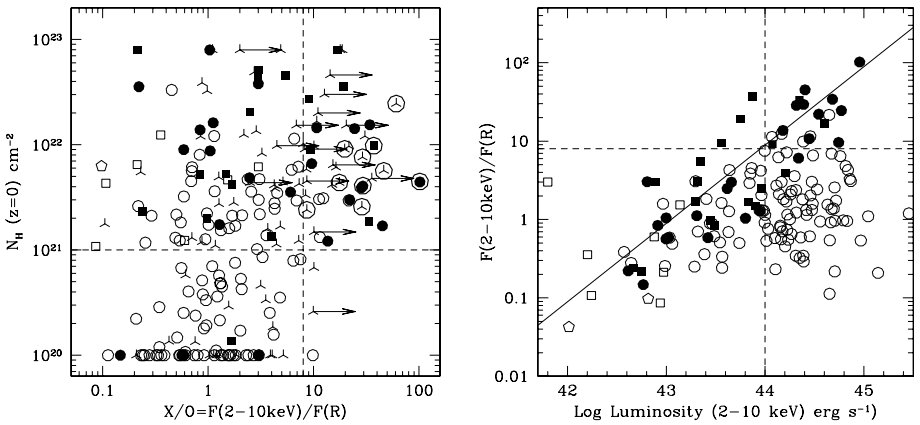

Fig. 4. The observed-frame absorbing column $N_{\rm H}(z = 0)$ as a function of the X-ray (2–10 keV) to optical (*R*-band) flux ratio X/O (*left panel*) and the X/O ratio as a function of the 2–10 keV luminosity (*right panel*) for the HELLAS2XMM full sample. Open circles = broad-line AGN; filled circles = narrow-line AGN; filled squares = emission-line galaxies; open squares = early-type galaxies; pentagons = groups/clusters of galaxies; skeleton triangles = unidentified objects. The 10 encircled symbols in the left panel have extreme $R - K$ colors ($R - K > 5$, see Mignoli et al. 2004). The diagonal line, in the right panel, is the best linear regression between log (X/O) and log L(2–10 keV) (from Fiore et al. 2003). The dashed lines represent the loci of constant $N_{\rm H} = 10^{21}$ cm^{-2}, X/O = 8 and log L(2–10 keV) = 44.

have a spectroscopic redshift[5]: in the following analysis we assume that the fraction of optically obscured AGN in these faint sources is similiar to the fraction in the HELLAS2XMM sample, i.e. a fraction of 0.76 ± 0.25. Assuming the fraction of optically obscured QSOs, it is possible to compute their integral number counts relations that are compared with the $\log N - \log S$ of the entire samples in Fig. 5b. Number counts and relative sky coverages are also tabulated in Table 2.

The line of reasoning followed to compute the fraction of optically obscured QSOs implies that the Fiore et al. (2003) relationship between X/O and log L(2–10 keV) may be directly applicable to the CDFS and CDFN sources with the faintest optical counterparts, assuming that also these sources are very likely high-luminosity objects, including them among the optically obscured QSO population. However, Bauer et al. (2004) and Barger et al. (2005) point out that the Fiore et al. (2003) relationship cannot be valid at faint ($R > 25.5$) optical magnitudes. For this reason, we re-computed the optically obscured QSO number counts by excluding all X-ray sources with optical counterparts fainter than $R = 25.5$ (open triangles in Fig. 5b). This is probably a lower limit to the "true" type 2 QSO surface density. In summary, we find a highly obscured QSO density of 45 ± 15 and 100–350 deg^{-2} at flux limits of 10^{-14} and 10^{-15} erg cm^{-2} s^{-1}, respectively (see Fig. 5b). The fraction of obscured QSOs to the total number of X-ray sources selected in the 2–10 keV band is therefore ~13% and between 4–14% at the two flux limits.

[5] To optically classify the CDFS and CDFN identified sources we applied our classification criteria where possible. The X-ray fluxes are taken from Alexander et al. (2003). The catalog reports 2–8 keV fluxes converted to 2–10 keV fluxes using a power-law model with spectral energy index $\alpha_E = 0.8$.

3.2. X-ray bright optical normal galaxies

In Fig. 6 we show the *R*-band images of the XBONG candidates with the largest X-ray to optical position difference. Superimposed are the X-ray position error boxes and the X-ray contours.

Close to the X-ray position of A1835_140 there are 2 optically bright sources, one within 3″ of the X-ray centroid and the other at 6.6″. Both sources are clearly extended and their morphology is consistent with a spheroid (see Civano et al. 2007, in preparation, for further details). The X-ray contours are centered on the source we identified as the optical counterpart of the X-ray source.

The *R*-band images of PKS0312_17 (H2XMMJ031124.8-770139) and PKS0312_501 (H2XMMJ030952.2-764927) are reported in the bottom panels; the optical counterpart identified for PKS0312_17 lies at 4.6″ from the nominal X-ray centroid but is coincident with a relatively bright radio source (see Brusa et al. 2003, for details). We therefore consider this optical source as the most likely counterpart of the X-ray source. As we can see in Fig. 6, the X-ray centroid of PKS0312_501 provided by the detection alghorithm is shifted slightly from the peak of the

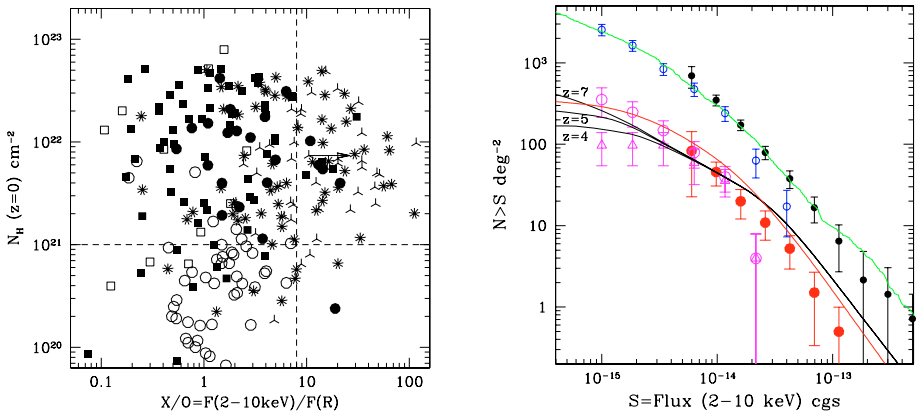

Fig. 5. a) *Left panel*: the observed-frame absorbing column $N_H(z = 0)$ as a function of the X-ray (2–10 keV) to optical (R-band) flux ratio X/O for the CDFS and CDFN samples. Open circles = broad-line AGN; filled circles = narrow-line AGN; filled squares = emission-line galaxies; open squares = early-type galaxies; pentagons = groups/clusters of galaxies; skeleton triangles = unidentified objects. The stars are sources with a photometric redshift. The dashed lines represent the loci of constant $N_H = 10^{21}$ cm^{-2} and X/O = 8. **b)** *Right panel*: the X-ray (2–10 keV) integral number counts from the HELLAS2XMM (filled symbols) and CDFS+CDFN samples (open symbols). The upper points are the number counts of the full samples, the solid curve is from the Moretti et al. (2003) compilation. The lower points refer to high-luminosity ($\log L$(2–10 keV) > 44), highly obscured sources only. Open triangles include only sources with optical counterparts brighter than $R = 25.5$. Black continuous lines represent the expected number counts from the Comastri et al. (2001) pure luminosity evolution XRB synthesis models ($z = 4, 5, 7$ are the maximum redshift over which the integration of the XLF is performed); the red line represents the expected number counts from the La Franca et al. (2005) luminosity-dependent density evolution model.

Table 2. Number counts and sky coverage.

F(2–10 keV) (10^{-14} erg cm^{-2} s^{-1})	Sky-coverage (deg^2)	Tot. N.C. (deg^{-2})	QSO2 N.C. (deg^{-2})	QSO2 N.C. ($R < 25.5$) (deg^{-2})
		HELLAS2XMM		
11.3	1.39	5.7 ± 2.8	0.5 ± 0.5	
6.93	1.37	16 ± 5.1	1.6 ± 1.4	
4.25	1.25	38 ± 8.7	5.7 ± 3.1	
2.60	0.98	79 ± 15	12.0 ± 6.1	
1.60	0.5	170 ± 26	21.9 ± 11.3	
0.98	0.11	350 ± 53	50.1 ± 23.2	
0.60	0.015	700 ± 210	91.1 ± 73.0	
		CDFS+CDFN		
4.00	0.174	17 ± 9.9	–	–
2.16	0.174	63 ± 24	4.3 ± 4.6	4.3 ± 4.6
1.17	0.174	240 ± 50	43 ± 21	39 ± 19
0.63	0.174	475 ± 89	87 ± 43	65 ± 37
0.34	0.14	840 ± 140	162 ± 74	106 ± 58
0.18	0.07	1640 ± 250	272 ± 130	106 ± 58
0.10	0.06	2560 ± 410	388 ± 200	106 ± 58

X-ray contours, which coincides with the optical counterpart. We therefore also consider this identification as reliable.

A paper discussing these sources in more detail and presenting near-infrared imaging is in preparation (Civano et al. 2007, in preparation). As an example, Fig. 7 shows the spectra of 2 XBONGs, which we tentatively classify as early-type galaxies based on the strong red continuum and the absence of emission lines (however, note that these spectra do not cover the Hα transition).

3.3. [OIII] emission

The [OIII]λ5007 line falls in the observed wavelength range for 59 of the 159 optical spectra of the full HELLAS2XMM sample. We measured[6] significant [OIII]λ5007 emission in 49 cases: 26 broad-line AGNs and 23 narrow-line AGNs (including 8 objects with optical spectra classified as emission-line galaxies but with 2–10 keV luminosity higher than 10^{42} erg s^{-1}). In the remaining 10 cases – 7 candidate XBONGs and 3 galaxies belonging to groups or small clusters of galaxies – we computed the 3σ upper limits (see Table 3).

Figure 8a shows the [OIII]λ5007 flux as a function of the 2–10 keV flux, while Fig. 8b shows the rest-frame N_H (computed using flux ratios, see Fiore et al. 2003) as a function of the ratio between the 2–10 keV and the [OIII]λ5007 luminosities for the 59 objects. Note that the XBONG candidates, in Fig. 8a, have systematically lower [OIII] fluxes compared to other sources with the same X-ray flux and have $L_{2-10\ \mathrm{keV}}/L_{[\mathrm{OIII}]} \gtrsim 1000$.

The only other HELLAS2XMM AGN with the X-ray-to-[OIII] luminosity ratio well above this value is the broad-line AGN A2690_3[7], a Seyfert 1 galaxy at $z = 0.433$ with strong broad MgII and H$_\beta$ lines but very faint [OIII] emission. Three other HELLAS2XMM AGN have $L_{2-10\ \mathrm{keV}}/L_{[\mathrm{OIII}]} \sim 1000$. This suggests that AGNs with small [OIII] emission are

[6] The [OIII]λ5007 fluxes were measured with a Gaussian fit of the line using the standard IRAF task *splot*.

[7] See `http://www.bo.astro.it/~hellas/sample.html`

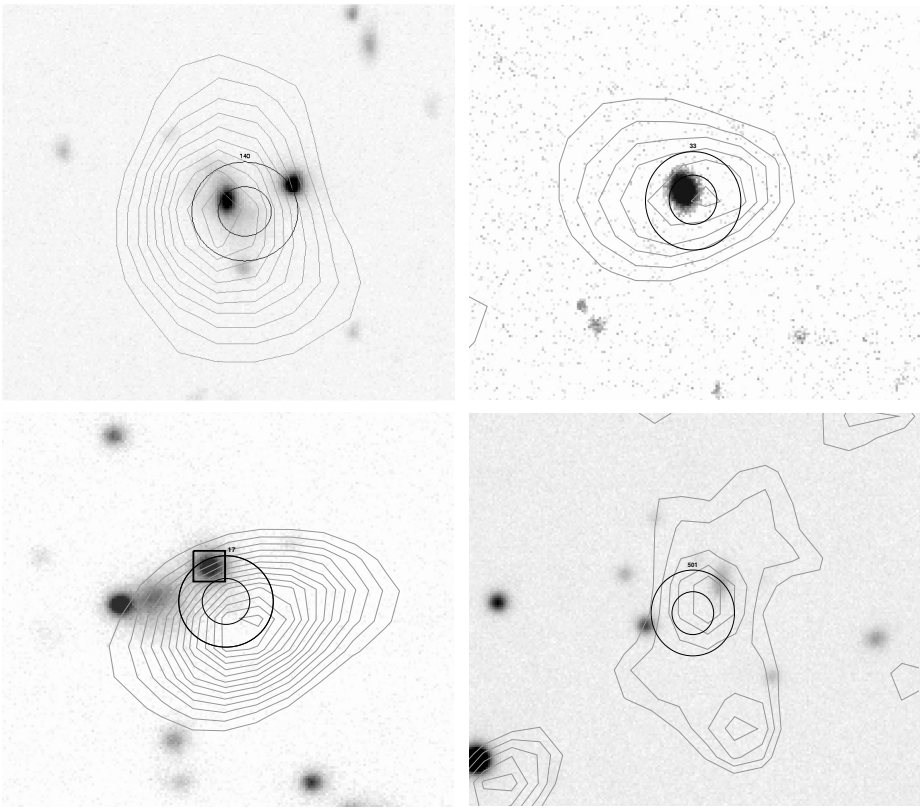

Fig. 6. *Upper panels*: the *R*-band images of A1835_140 (H2XMMJ140144.9+025332, *left*) and A1835_33 (H2XMMJ140057.3+023942, *right*). Superimposed are the X-ray position error boxes (3″ and 6″ black circles) and the X-ray contours (grey). The X-ray contours are centered on the sources identified by us as the optical counterpart of the X-ray sources. *Bottom panels*: the *R*-band images of PKS0312_17 (H2XMMJ031124.8-770139, *left*) and PKS0312_501 (H2XMMJ030952.2-764927, *right*): the optical counterpart identified for PKS0312_17 is coincident with a relatively bright radio source (the square refers to the radio centroid, 4″ width, see Brusa et al. 2003). The X-ray centroid of PKS0312_501 is slightly shifted from the peak of the X-ray contours, which are coincident with the optical countepart. We therefore also consider this indentification as reliable.

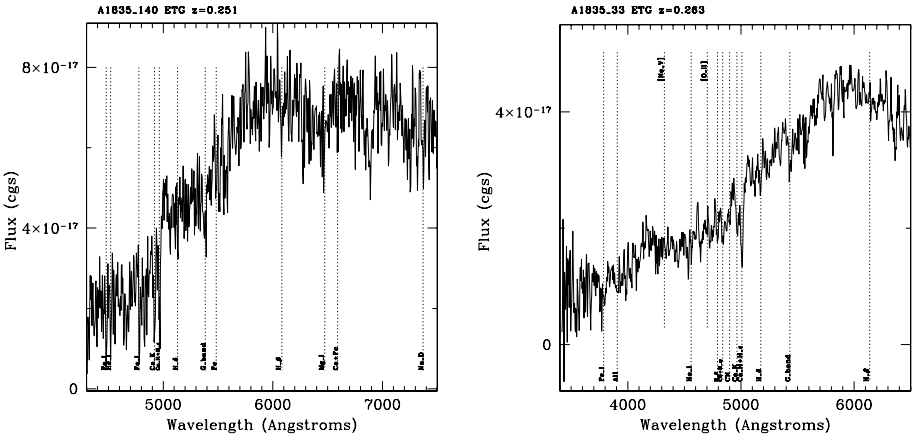

Fig. 7. The optical spectra of A1835_140 (H2XMMJ140144.9+025332, $z = 0.251$) and A1835_33 (H2XMMJ140057.3+023942, $z = 0.263$). Note the strong Balmer breaks, red continua and absence of strong [OII] and [OIII] emission lines.

probably more common than what was thought before and that the XBONGS are the tip of the iceberg for this source population.

4. Discussion

The hard X-ray selection and the good photometric and spectroscopic coverage of the ten HELLAS2XMM fields allow us to probe AGN activity over a wide range of broad band properties. We focus our attention on two extremes of the AGN activity: on one side, sources with a high X-ray-to-optical flux ratio, the majority of which turned out to be the thus far "elusive" high-luminosity, highly obscured type 2 QSOs; at the other end, sources with relatively low X-ray-to-optical flux ratios, moderately luminous ($L_X \simeq 10^{42-43}$ erg s^{-1}) active nuclei in otherwise inactive galaxies, the so-called XBONGs.

4.1. The high X/O flux ratio sources

We confirm the finding that about 20% of hard X-ray selected sources have an X-ray-to-optical flux ratio which is, on average, one order of magnitude or more higher than that of optically selected AGNs. Our spectroscopic identifications suggest that ∼76% of the sources with X/O > 8 and $\log N_H(z = 0) > 21$ are highly obscured QSOs at $z = 0.7$–2 (see also Table 1). This implies a number density of optically obscured QSOs of ∼45 deg^{-2} at a flux limit of 10^{-14} erg cm^{-2} s^{-1}. Within the reasonable hypothesis that the fraction of obscured QSOs among the sources with X/O > 8 and $\log N_H(z = 0) > 21$ remains constant down to fluxes of 10^{-15} erg cm^{-2} s^{-1}, an obscured QSOs density of ∼350 deg^{-2} is implied. A much more conservative estimate of the obscured QSO space density (∼100 deg^{-2} at 10^{-15} erg cm^{-2} s^{-1}), which should probably be considered as a lower limit, is obtained by assuming that all sources with optical counterparts fainter than $R = 25.5$ have X-ray luminosities below the highly obscured QSO threshold.

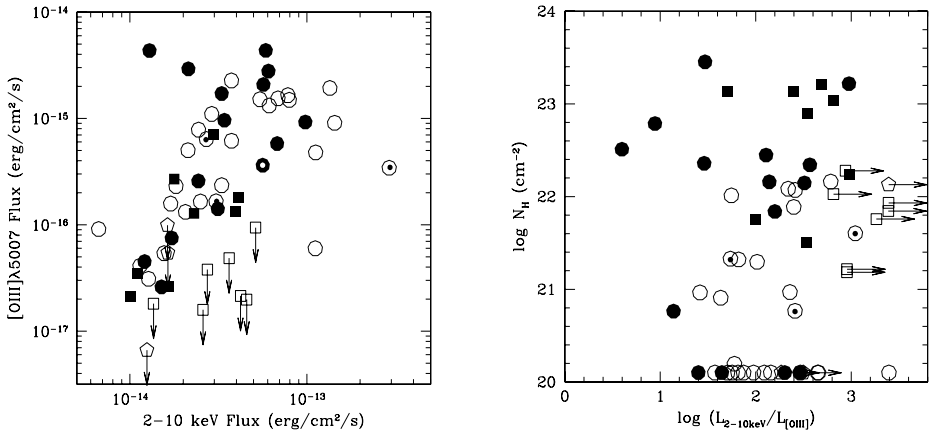

Fig. 8. a) *Left panel*: the [OIII]λ5007 flux as a function of the 2–10 keV flux for 59 sources of the full HELLAS2XMM sample. **b)** *Right panel*: the rest-frame absorbing column density $N_{\rm H}$ (computed using flux ratios) as a function of the ratio between the 2–10 keV luminosity and the [OIII]λ5007 luminosity. Open circles = broad-line AGN; filled circles = narrow-line AGN; filled squares = emission-line galaxies; open squares = early-type galaxies; pentagons = groups/clusters of galaxies; skeleton triangles = unidentified objects. The four encircled symbols in both panels mark objects for which the [OIII]λ5007 line lies within strong telluric absorption features.

The three black solid curves in Fig. 5b superimposed on the number counts of high-luminosity, highly obscured objects from both HELLAS2XMM and CDFS+CDFN samples are the number counts of obscured QSO predicted by the Comastri et al. (1995, 2001) XRB synthesis models. These models assume an evolution of the X-ray luminosity function parameterized by a pure luminosity evolution (PLE) law [$L(z) \propto L(z = 0) \times (1 + z)^{2.6}$] up to $z = 1.5$ and constant up to a maximum redshift $z_{\rm max}$ ($z_{\rm max}$ = 4, 5, 7; see Fig. 5b). These predictions (also depending on the adopted maximum redshift) lie in between the two number counts obtained by assuming that 70% of the high X/O sources are obscured QSOs or including in the obscured QSO sample sources with optical counterparts brighter than $R = 25.5$ only, respectively. The red curve in the Fig. 5b represents the prediction obtained by the luminosity dependent density evolution (LDDE) model of the hard X-ray luminosity function described in La Franca et al. (2005). Not surprisingly, the shape of the number counts relations obtained by integrating the PLE and the LDDE models are different. The latter slightly overpredicts the highly obscured QSO number counts at fluxes $\gtrsim 10^{-14}$ erg cm^{-2} s^{-1}, while at lower fluxes it agrees pretty well with the expectations based on the identification of obscured QSOs with 70% of the high X/O sources (see Sect. 3.1). The same model predicts that the number of obscured QSO with $\log L(2\text{–}10\ {\rm keV}) > 44$ is comparable to that of unobscured QSO. A similar conclusion was found by Perola et al. (2004) using a smaller source sample (the HELLAS2XMM 1dF sample). However, most of these hard X-ray selected, highly obscured QSOs have column densities in the range $N_{\rm H} \sim 10^{22-23}$ cm^{-2} with only a handful of the faintest sources that could be Compton thick ($N_{\rm H} > 10^{24}$ cm^{-2}). According to the most recent version of the AGN synthesis models for the X-ray background (Gilli et al. 2007), the fraction of Compton-thick AGN in deep XMM-*Newton* and *Chandra* surveys is expected to be at most a few percent. Indeed, Tozzi et al. (2006) find that only about 4% of the sources in the CDFS have a 0.5–8 keV spectrum consistent with Compton-thick absorption and/or pure reflection. Therefore, we still may be viewing just the tip of the iceberg of highly obscured sources at high-redshift.

An approach to find highly obscured, Compton-thick QSOs is to select sources with QSO luminosities in the mid-infrared band and with faint or extremely faint near-infrared and optical counterparts. Martinez-Sansigre et al. (2005) estimate that probably more than half of the high-luminosity QSOs are highly obscured, although with large uncertainties. Unfortunately, the X-ray properties of infrared selected sources are not known, making it difficult to understand how the mid-infrared selection compares with the X-ray one. In particular, it is not clear what the fraction is of the mid-infrared-selected, highly obscured QSOs that would have been selected by hard X-ray surveys and whether the mid-infrared selection is truly more efficient for discovering Compton-thick sources.

To answer to these questions we can take advantage of the study of fields with both X-ray and mid-infrared coverage; for example, we are analyzing the Spitzer observations of 12 HELLAS2XMM sources (Pozzi et al., in preparation). Furthermore, the study of the ELAIS-S1 (Puccetti et al. 2006) and the COSMOS fields and/or deep X-ray follow-up observations of the mid-infrared selected sources in the Spitzer First Look Survey (Martinez-Sansigre et al. 2005) will certainly bring new light on this topic.

4.2. XBONGs

At the other extreme of the X-ray-to-optical flux ratio distribution, we find the other class of "elusive" AGN (i.e., XBONGs), objects whith Seyfert-like X-ray luminosities but without any signature of nuclear activity in either optical imaging or spectroscopy (Comastri et al. 2002; Moran et al. 2002; Severgnini et al. 2003). In order to provide a quantitative definition of these objects, the flux and luminosity of the [OIII]λ5007 emission (or their upper limits) are measured for the 59 spectra in the full HELLAS2XMM sample that covers this transition.

The HELLAS2XMM AGNs with [OIII] detection have a $L_{2-10\ {\rm keV}}/L_{\rm [OIII]}$ ratio between 3 and 1000 with a logarithmic median of 2.14 and interquartile range 0.38. This is systematically higher than optically selected sources. As an example, unobscured PG quasars at $z < 0.4$ have $L_{2-10\ {\rm keV}}/L_{\rm [OIII]}$ in the range 6–500 (Laor et al. 1997), Compton-thin, Seyfert 2 galaxies have $L_{2-10\ {\rm keV}}/L_{\rm [OIII]}$ between 3 and 50, while Compton-thick Seyfert 2 galaxies have $L_{2-10\ {\rm keV}}/L_{\rm [OIII]}$ between 0.03 and 1 (Maiolino et al. 1998; Bassani et al. 1999). All the HELLAS2XMM AGNs have $L_{2-10\ {\rm keV}}/L_{\rm [OIII]} > 3$ and therefore, as discussed above, no Compton-thick object ($\log N_{\rm H} \gtrsim 24$) is likely to be present in the HELLAS2XMM sample. The discrepancy between the $L_{2-10\ {\rm keV}}/L_{\rm [OIII]}$ ratio of the HELLAS2XMM AGN and optically selected AGNs could be due to the fact that the [OIII] luminosity of the HELLAS2XMM AGN is not corrected for reddening. This correction can be very large for highly obscured sources. Indeed, the typical correction in Bassani et al. (1999) is a factor between 2 and 10, with a few extreme objects having a correction approaching 50. The logarithmic median $L_{2-10\ {\rm keV}}/L_{\rm [OIII]}$ and its interquartile range of a sample of 24 Compton-thin,

narrow-line AGNs from the catalogs of Maiolino & Rieke (1995) and Bassani et al. (1999), obtained without correcting for extinction, plus 17 PG quasar from the Laor et al. (1997) sample (41 sources in total), is 1.69 and 0.30, lower than the median of the HELLAS2XMM sources. The probability that the two $\log L_{2-10\ \mathrm{keV}}/L_{[\mathrm{OIII}]}$ distributions are drawn from the same parent population is 1.8%, using the Kolmogorov-Smirnov test. The higher $L_{2-10\ \mathrm{keV}}/L_{[\mathrm{OIII}]}$ ratio of X-ray selected AGN with respect to optically selected AGN is intriguing, because it suggests that these samples are at least partly incomplete, and that [OIII] emission is not a perfect isotropic indicator of the nuclear power. However, this must be confirmed by using larger samples with both good X-ray and [OIII] determinations.

Narrow-line AGNs tend to have higher column densities than broad-line AGNs, but we do not see any correlation between the column density and $L_{2-10\ \mathrm{keV}}/L_{[\mathrm{OIII}]}$ (see Fig. 8b). On the other hand, XBONG candidates have lower [OIII] fluxes compared with the other sources with similiar X-ray flux (see Fig. 8a) and have $L_{2-10\ \mathrm{keV}}/L_{[\mathrm{OIII}]} \gtrsim 1000$ (see Fig. 8b). This suggests that the $L_{2-10\ \mathrm{keV}}/L_{[\mathrm{OIII}]}$ ratio is a robust index for defining X-ray bright but optically normal galaxies (XBONGs), at least in the X-ray and [OIII] flux ranges covered by the present observations. Note that this classification criterion is nearly independent of the galaxy dilution of the nuclear spectrum, which has been suggested as the key ingredient in the classification of XBONGs (see Severgnini et al. 2003; Moran et al. 2002; Georgantopoulos & Georgakakis 2005), since it is related to a direct measurement of the line flux and not to its equivalent width. Indeed, the main issue about the XBONGs nature is whether they are just typical AGNs (in terms of both X-ray and line emission luminosity) or, rather, they represent a truly distinct class. Our results strongly point towards the latter hypothesis.

To investigate this issue further, we compared the 7 XBONG candidates to 7 narrow-line AGNs found in the same redshift interval (0.075–0.32). XBONGs and narrow-line AGNs have very similar X-ray luminosity (median $\log L(2\text{–}10\ \mathrm{keV}) = 42.94$ vs. 42.76), optical luminosity (median $L(R) = 10.60$ vs. $10.77\ L_{\odot}$), X-ray-to-optical flux ratio (median X/O = 0.35 vs. 0.26), and absorbing column densities (median $\log N_{\mathrm{H}} = 21.8$ vs. 21.6). On the other hand, while the narrow-line AGNs have median [OIII]λ5007 flux and luminosity of 9.2×10^{-16} erg cm^{-2} s^{-1} and 1.6×10^{41} erg s^{-1}, XBONGs have 3σ upper limits in the ranges $1.5\text{–}9.4 \times 10^{-17}$ erg cm^{-2} s^{-1} and $2.5 \times 10^{38}\text{–}1.4 \times 10^{40}$ erg s^{-1}, i.e., 10–50 times lower than narrow-line AGNs. These findings suggest that, while the central engine of narrow-line AGNs and XBONGs is likely to be the same, narrow emission lines in XBONGs are strongly inhibited or obscured.

At least three possibilities are envisaged to explain the lack of optical line emission:

- 1) the physical size of the narrow emission-line region could be reduced with respect to normal AGNs, or even absent (see, e.g., Hawkins 2004);
- 2) the optical-UV nuclear continuum could be screened by circumnuclear absorbing gas and dust covering a large solid angle at the nuclear engine, so that the ionizing radiation does not (or only partially) reach the narrow emission-line clouds;
- 3) the emission lines could be quenched by obscuring dust spatially distributed on larger scales (i.e., kpc dust lanes) as observed in HST images of nearby Seyfert 2 galaxies (Malkan et al. 1998).

To disentangle these hypotheses, we are pursuing an intensive multiwavelength observing strategy, including more high angular resolution X-ray imaging with *Chandra* and spatially-resolved optical spectroscopy with the VIMOS Integral Field Unit at VLT.

5. Conclusions

We have obtained optical photometry and spectroscopy for a sample of 110 sources detected in the 2–10 keV band in five additional XMM-*Newton* fields of the HELLAS2XMM serendipitous survey, covering an additional 0.5 deg^2 of the sky at the bright flux limit (see Table 2). We report the spectroscopic identification of 59 new redshifts, bringing to 159 the total number of X-ray sources with redshift identifications in the full HELLAS2XMM sample (including the three near-infrared spectroscopic redshifts reported by Maiolino et al. 2006).

Combining the redshift information of the HELLAS2XMM sample with what is available in the CDFS and CDFN surveys, the fraction of highly obscured type 2 QSOs is estimated to be on the order of ∼13% of the total, which is fairly independent of the X-ray flux for $F(2\text{–}10\ \mathrm{keV}) > 10^{-15}$ erg cm^{-2} s^{-1}. This result roughly agrees with the Comastri et al. (2001) and La Franca et al. (2005) models and implies that about half of the luminous AGNs ($\log L(2\text{–}10\ \mathrm{keV}) > 44$) are obscured.

We find that the 7 XBONG candidates in the full HELLAS2XMM sample have $L_{2-10\ \mathrm{keV}}/L_{[\mathrm{OIII}]} \gtrsim 1000$, while all but one of the other HELLAS2XMM AGNs have an X-ray-to-[OIII] ratio well below this value. Although the sample is very small and, therefore, subject to large uncertainties, our results suggest that this ratio can be used to efficiently select XBONG candidates. Multiwavelength works with further surveys are needed to strengthen this result.

Acknowledgements. This research has been partially supported by ASI, INAF–PRIN 270/2003, and MIUR Cofin-03-02-23 grants. We acknowledge an anonymous referee for comments that improved the presentation. We thank L. Pentericci, P. Tozzi, and P. Severgnini for useful discussions.

References

Alexander, D. M., Bauer, F. E., Brandt, W. N., et al. 2003, AJ, 126, 539
Baldi, A., Molendi, S., Comastri, A., et al. 2002, ApJ, 564, 190
Banse, K., Crane, P., Grosbol, P., et al. 1983, The Messanger, 31, 26
Bassani, L., Dadina, M., Maiolino, R., et al. 1999, ApJS, 121, 473
Barger, A. J., Cowie, L. L., Capak, P., et al. 2003, AJ, 126, 632
Barger, A. J., Cowie, L. L., Mushotzky, R. F., et al. 2005, AJ, 129, 578
Bertin, E., & Arnouts, S. 1996, A&AS, 117, 393
Bauer, F. E., Alexander, D. M., Brandt, W. N., et al. 2004, AJ, 128, 2048
Brandt, W. N., & Hasinger, G. 2005, ARA&A, 43, 1056
Brusa, M., Comastri, A., Mignoli, M., et al. 2003, A&A, 409, 65
Civano, et al., in preparation
Comastri, A. 2004, in Supermassive Black Holes in the Distant Universe, ed. A. J. Barger (Kluwer Academic), 308, 245
Comastri, A., Setti, G., Zamorani, G., & Hasinger, G. 1995, A&A, 296, 1
Comastri, A., Fiore, F., Vignali, C., et al. 2001, MNRAS, 327, 781
Comastri, A., Mignoli, M., Ciliegi, P., et al. 2002, ApJ, 571, 771
Croom, S. M., Boyle, B. J., Loaring, N. S., et al. 2002, MNRAS, 335, 459
Della Ceca, R., Maccacaro, T., Caccianiga, A., et al. 2004, A&A, 428, 383
Eckart, M. E., Laird, E. S., Stern, D., et al. 2005, ApJS, 156, 35
Eckart, M. E., Stern, D., Helfand, D., et al. 2006, ApJS, 165, 19
Fiore, F. 2004, NuPhS, 132, 69
Fiore, F., La Franca, F., Vignali, C., et al. 2000, NewA, 5, 143
Fiore, F., Brusa, M., Cocchia, F., et al. 2003, A&A, 409, 79
Georgakakis, A., Georgantopoulos, I., Vallbé, M., et al. 2004, MNRAS, 349, 135
Georgantopoulos, I., & Georgakakis, A. 2005, MNRAS, 358, 131
Giacconi, R., Zirm, A., Wang, J., et al. 2002, ApJS, 139, 369
Gilli, R., Comastri, A., & Hasinger, G. 2007, A&A, 463, 79

Hasinger, G. 2003, proceedings of the Conference: The Emergence of Cosmic Structure, Maryland, ed. S. S. Holt, & C. Reynolds [arXiv:astro-ph/0302574]
Hasinger, G., Burg, R., Giacconi, R., et al. 1998, A&A, 329, 482
Hawkins, M. R. S. 2004, A&A, 424, 519
Kauffmann, G., Heckman, T. M., Tremonti, C., et al. 2003, MNRAS, 346, 1055
La Franca, F., Fiore, F., Comastri, A., et al. 2005, ApJ, 635, 864
Laor, A., Fiore, F., Elvis, M., et al. 1997, ApJ, 477, 93
Maccacaro, T., Gioia, I., Wolter, A., et al. 1988, ApJ, 326, 680
Mainieri, V., Bergeron, J., Hasinger, G., et al. 2002, A&A, 393, 425
Maiolino, R., & Rieke, G. H. 1995, ApJ, 454, 95
Maiolino, R., Salvati, M., Bassani, L., et al. 1998, A&A, 338, 781
Maiolino, R., Mignoli, M., Pozzetti, L., et al. 2006, A&A, 445, 457
Malkan, M. A., Gorjian, V., & Tam, R. 1998, ApJ, 117, 25
Martinez-Sansigre, A., Rawlings, S., Lacy, M., et al. 2005, Nature, 436, 666
Mignoli, M., Pozzetti, L., Comastri, A., et al. 2004, A&A, 418, 827
Mineo, T., Fiore, F., Laor, A., et al. 2000, A&A, 359, 471
Moran, E. C., Filippenko, A. V., & Chornock, R. 2002, ApJ, 579, L71
Moretti, A., Campana, S., Lazzati, D., & Tagliaferri, G. 2003, ApJ, 588, 696
Perola, G. C., Puccetti, S., Fiore, F., et al. 2004, A&A, 421, 491
Puccetti, S., Fiore, F., D'Elia, V., et al. 2006, A&A, 457, 501
Oke, J. B. 1990, AJ, 99, 1621
Severgnini, P., Caccianiga, A., Braito, V., et al. 2003, A&A, 406, 483
Silverman, J. D., Green, P. J., Barkhouse, W. A., et al. 2005, ApJ, 618, 123
Steffen, A. T., Barger, A. J., Capak, P., et al. 2004, AJ, 128, 1483
Szokoly, G. P., Bergeron, J., Hasinger, G., et al. 2004, ApJS, 155, 271
Tozzi, P., Gilli, R., Mainieri, V., et al. 2006, A&A, 451, 457
Treister, E., Castander, F. J., Maccarone, T. J., et al. 2005, ApJ, 621, 104
Ueda, Y., Takahashi, T., Ishisaki, Y., & Ohashi, T. 1999, ApJ, 524L, 11
Worsley, M. A., Fabian, A. C., Barcons, X., et al. 2004, MNRAS, 352, L28
Zakamska, N. L., Strauss, M. A., Krolik, J. H., et al. 2003, AJ, 126, 2125